The Effect of Low-Filler Volume Fraction on the Elastic Modulus and Thermal Expansion Coefficient of Particulate Composites Simulated by a Multiphase Model

E. Sideridis, V. N. Kytopoulos, G. A. Papadopoulos, G. D. Bourkas

Laboratory of Strength and Materials, Department of Mechanics, Faculty of Applied Sciences, National Technical University of Athens, Athens, Greece

Received 6 November 2007; accepted 14 January 2008
DOI 10.1002/app.28886
Published online 3 October 2008 in Wiley InterScience (www.interscience.wiley.com).

ABSTRACT: The aim of this investigation is to determine the effect of low-filler volume fraction on the elastic modulus and the thermal expansion coefficient of particulate composites. In the theoretical part, theoretical model valid for low-filler volume fractions is used to evaluate these two magnitudes. In the experimental part, low-percentage filler contents of 3, 5, 7, and 10% are used. The density for these epoxy resin-iron particle composites is also determined. At the same time, an attempt to explain some of the disagreements observed between theoretical values and experimental data on a qualitative basis is also made. This attempt is in part assisted by scanning electron microscopy (SEM) observations concerning structural inhomogeneities and fractographical data. The comparison of the theoretical values derived from the present model with experimental results and with theoretical values derived from other workers appears satisfactory in many cases, but in some others the discrepancies among them are considerable. © 2008 Wiley Periodicals, Inc. J Appl Polym Sci 111: 203–216, 2009

Key words: particulate composites; thermal expansion coefficient; multiphase model

INTRODUCTION

The introduction of inclusions into a polymeric matrix results in the production of a composite material with superior stiffness and sometimes strength. However, prediction of the properties of the product is difficult, since they depend on a great number of structural parameters. Attempts to make such predictions may lead to a rough estimation of the influence of fillers on the overall behavior of the composite. For instance, the reinforcing action of the filler is limited by the nature, shape, size, and distribution of the filler, and on the other hand, by the adhesion efficiency between the two phases and the mechanism of microfailure of the composite system. Also, another important factor affecting the strength properties is the interaction between individual filler particles. This last parameter is difficult to predict in a real composite.[1]

As mentioned, the adhesion bond between polymer and inclusion is an important factor affecting very much the strength and the stiffness of a particulate composite. By the term adhesion, we are referred to the energy of interaction at the interface. For instance, a proper surface treatment of the filler particles can lead to a better adhesion between polymer and inclusion and, consequently to a change in the overall mechanical behavior of the composite system. It is well known that in the region between matrix and inclusion, a third phase, an interphase is developed consisting of areas of imperfect adhesion stress because of the concentrations of impurities and other microdefects.[2] All these imperfections may lead to localized stress concentrations, which are in excess of the average stress in the bulk of the material. If the localized stresses are sufficiently high, they may lead to a microcrack growth of the defect and thus to a premature failure of the material. In this sense, the rate of microcrack growing depends strongly on the degree of structural inhomogeneity of the material, not only in the macroscopic sense of the term but rather on its microscopic sense. This is due to the presence of filler that influences the structure formation.[3]

From the aforementioned observations, it becomes clear that the filler volume fraction plays a very important role on the mechanical behavior of the particulate composites.

However, one of the important problems remains the prediction of the composite properties from the properties of the constituent materials. The difficulty

Correspondence to: G. A. Papadopoulos (gpad@central.ntua.gr).

of this problem arises from the fact that, for example, the thermomechanical properties of a composite material may depend on several structural parameters, such as the individual properties of the filler and the matrix, the particle size and distribution, the filler volume fraction, the quality of adhesion between filler and matrix, the influence of neighboring particles, the mode of filler-packing, and other structural inhomogeneities.

The various theoretical models that have been proposed[4–16] to predict the mechanical properties of composites have emphasized particular parameters. The filler-volume fraction and the mode of packing were the parameters studied in the model presented in Refs. 4–6, whereas the importance of the particle size on the final properties of the composites was discussed in Refs. 7–11. The effect of the filler-matrix adhesion on the mechanical behavior of composites has been discussed in a series of models presented in Refs. 1–3 and 11–16. A number of theoretical analyses that define the thermal properties of composites and give equations for predicting the thermal expansion coefficient have been reported in the literature.[17–27] Some of these equations have been verified experimentally for some practical systems, but for other systems poor agreement was found between theoretical and experimental results. Excellent review articles and mathematical treatments based on energy principles can be found in the literature. It has been realized that a state of microstress often exists between the phases. Differences in the thermal expansivities of the individual phases produce stresses, the existence of which has been demonstrated directly by X-ray diffraction and indirectly through their effect on the strength properties and modes of failure. These stresses influence the thermal expansion behavior of the composite body. In Ref. 15 it was demonstrated experimentally that the thermal expansion coefficient did not obey the law of mixtures as also reported earlier in Refs. 17 and 25.

In this article, a five-phase (pentaphase) theoretical model for the evaluation of the elastic modulus and thermal expansion coefficient, which is valid only for low-filler volume fractions of particulate composites, was developed. In the experimental part, different low-percentage filler contents $U_f = 0$, 0.03, 0.05, 0.07 and 0.10 were used.

A comparison of the theoretical values obtained from the present model with experimental results and with theoretical values given by other authors is also carried out.

Finally, a qualitative explanation concerning the observed discrepancies between values from theoretical models and experimental results on the basis of certain structural inhomogeneities and microfailure data obtained by scanning electron microscopy (SEM) fractography is given.

THEORETICAL ANALYSIS

The proposed model

The aim of microstructural composite models is to reproduce the basic cell or the representative volume element of the composite at a macroscopic scale in order that a respective experimental solution to be obtained with problems not susceptible to analytical treatment.

The microstructural models are usually based on the following assumptions:

i) A regular geometric form is adopted for the inclusions usually a sphere or cylinder.
ii) Regular geometry and topology are adopted for the model.

The adopted spatial model is presented in Figure 1(a). It represents fully a three-dimensional system capable of simulating real particle composites. Assuming equal fillers, the volume fraction U_f, f the filler in the continuous matrix is given in terms of the ratio $2r_f/\ell$, where r_f is the filler radius and ℓ the side.

To make a more refined analysis, a 12-face (dodecahedric) model is adopted as basis. It has 12 faces, 30 sides of length ℓ, and 20 corners (vertices). The total volume is given as $V = (15 + 7\sqrt{5})\ell^3/4$ (with $K_1 = (15 + 7\sqrt{5})/4$),

the surface of each face

$$S = (3\sqrt{25 + 10\sqrt{5}})/\ell^2$$

and each angle $\varphi = 116^\circ\ 34'$.

The radius of the described sphere is

$$R_1 = \ell\sqrt{3}(\sqrt{5} + 1)/4 = 1.4013\ \ell,$$

that of the inscribed sphere

$$R_2 = (\ell\sqrt{250 + 110\sqrt{5}})/20 = 1.1135\ \ell$$

and the distance of the mass center from the mid-distance of each side is $R_3 = 1.3090\ell$. Then, three models can be taken into consideration as derived from the following combinations:

(i) A dodecahedron with $N_1 = 30$ inclusions of the middle of its sides and $N_1' = 20$ inclusions at the corners. This model is designated as M_1.
(ii) A dodecahedron with $N_2 = 12$ inclusions at the center of its faces and $N_2' = 20$ inclusions at the corners. This model is designated as M_2.

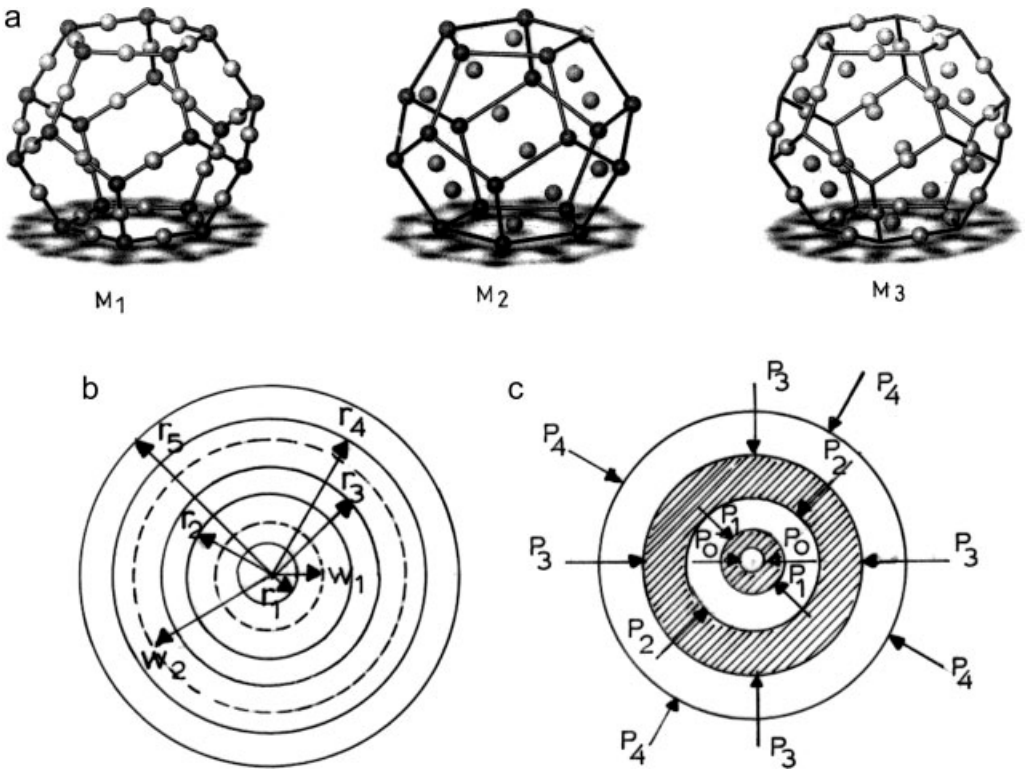

Figure 1 (a) Proposed spatial model of the composite material. (b) Proposed model for the theoretical analysis. (c) Schematic representation of the stresses.

(iii) A dodecahedron with $N_3 = 12$ inclusions at the center of its faces and $N_3' = 30$ inclusions at the middle of its sides. This model is designated as M_3.

A dodecahedron with side length 2ℓ is assumed to form the unit cell of the composite. This is transformed to a spherical representative volume element (RVE) according to the following assumptions:

(i) A sphere with radius r_1 that simulates the matrix in the dodecahedron of side ℓ.
(ii) A concentric hollow sphere of radii r_1 and r_2 that simulates the N_i ($i = 1,2,3$) inclusions in the dodecahedron.
(iii) A concentric hollow sphere of radii r_2 and r_3 that simulates the remaining matrix, which extends up to the corners of the dodecahedron of side ℓ.
(iv) A concentric hollow sphere of radii r_3 and r_4 that simulates the N_i' ($i = 1,2,3$) inclusions in the dodecahedron.
(v) A sphere with radius r_5 having equal volume with the dodecahedron of side 2ℓ.

The concentric hollow sphere of radii r_4 and r_5 simulates the remaining matrix that extends up to the corners of the dodecahedron of side 2ℓ.

The following relationships can be written to calculate the radii r_1,r_2, r_3, r_4, r_5. The total volume fraction is given as follows:

$$U_f = \frac{N_i\left(\frac{4}{3}\pi\, r_f^3\right) + N_i'\left(\frac{4}{3}\pi\, r_f^3\right)}{K_1(2\ell)^3} = \frac{\left(N_i + N_i'\right)\frac{4}{3}\pi\, r_f^3}{K_1(2\ell)^3} \quad (1)$$

where N_i and N_i' ($i = 1,2,3$) were given previously.

For the equality of the volume dodecahedron of side 2ℓ and the outer sphere, we have

$$K_1(2\ell)^3 = \frac{4}{3}\pi\, r_5^3 \quad (2)$$

which by the aid of eq. (1) yields:

$$r_5 = r_f \sqrt[3]{\frac{\left(N_i + N_i'\right)}{U_f}} \quad (3)$$

By substituting ℓ from eq. (1) we obtain:

$$\ell = r_f \sqrt[3]{\frac{\left(N_i + N_i'\right)\pi}{6K_1 U_f}}$$

For model M_1, the distance of the center of the dodecahedron, of side ℓ, to the middle of one side is

TABLE I
Radii of the Adopted Models

Model	w_1	w_2
M_1	$1.3090 r_f \sqrt[3]{\frac{50\pi}{6K_1U_f}}$ (4a)	$1.4013 r_f \sqrt[3]{\frac{50\pi}{6K_1U_f}}$ (4b)
M_2	$1.1135 r_f \sqrt[3]{\frac{32\pi}{6K_1U_f}}$ (5a)	$1.4013 r_f \sqrt[3]{\frac{32\pi}{6K_1U_f}}$ (5b)
M_3	$1.1135 r_f \sqrt[3]{\frac{42\pi}{6K_1U_f}}$ (6a)	$1.3090 r_f \sqrt[3]{\frac{42\pi}{6K_1U_f}}$ (6b)

designated as w_1 and that of its center to one corner is designated as w_2. They are given as follows: $w_1 = 1.3090\ell$ and $w_2 = 1.4013\ell$.

For Model M_2, the distance of the center of the dodecahedron to the center of one face is designated as w_1 and that of its center to one corner as w_2. They are given as follows:

$$w_1 = 1.1135\ell \quad \text{and} \quad w_2 = 1.4013\ell.$$

Finally, for Model M_3, the distance of the center of the dodecahedron to the center of one face is designated as w_1 and that of its center to the middle of one side as w_2. They are given as follows:

$$w_1 = 1.135\ell \quad \text{and} \quad w_2 = 1.3090\ell.$$

By the substitution of ℓ, we obtain the following expression for w_1 and w_2 for each model (Table I):

Now, it is considered that the volume of the hollow spherical region with radii r_2 and r_3 is distributed in equal volume parts on both sides of spherical surface of radius w_1:

$$\frac{4}{3}\pi\left(r_2^3 - w_1^3\right) = \frac{4}{3}\pi\left(w_1^3 - r_1^3\right) \rightarrow r_1^3 + r_2^3 = 2w_1^3 \qquad (7)$$

However, the volume of the second region is equal to the volume of N_i (i = 1,2,3) inclusions according to each one of the adopted models, i.e., $N_1 = 30$ for Model M_1, $N_2 = 12$ for Model M_2, and $N_3 = 12$ for Model M_3. Thus,

$$\frac{4}{3}\pi\left(r_2^3 - r_1^3\right) = N_i\frac{4}{3}\pi\, r_f^3 \rightarrow r_2^3 - r_1^3 = N_i r_f^3 \qquad (8)$$

Also, it is considered that the volume of the hollow spherical region with radii r_3 and r_4 is distributed in equal volume parts on both sides of spherical surface of radius w_2:

$$\frac{4}{3}\pi\left(r_4^3 - w_2^3\right) = \frac{4}{3}\pi\left(w_2^3 - r_3^3\right) \rightarrow r_3^3 + r_4^3 = 2w_2^3 \qquad (9)$$

However, the volume of the fourth region is equal to the volume of N_i' (i = 1,2,3) inclusions according to each one of the adopted models, i.e., $N_1' = 20$ for Model M_1, $N_2' = 20$ for M_2, and $N_3' = 30$ for Model M_3. Thus:

$$\frac{4}{3}\pi\left(r_4^3 - r_3^3\right) = N_i\frac{4}{3}\pi\, r_f^3 \rightarrow r_4^3 - r_3^3 = N_i r_f^3 \qquad (10)$$

The solution of the system of eqs. (7–10) yields the values of radii r_1, r_2, r_3, r_4.

$$r_1 = \sqrt[3]{w_1^3 - \frac{N_i}{2}r_f^3}, \quad r_2 = \sqrt[3]{w_1^3 + \frac{N_i}{2}r_f^3},$$
$$r_3 = \sqrt[3]{w_2^3 - \frac{N_i'}{2}r_f^3}, \quad r_4 = \sqrt[3]{w_2^3 + \frac{N_i'}{2}r_f^3} \qquad (11a,b,c,d)$$

Now, an observation of the above expressions to check the validity of the proposed models reveals that r_2 and r_4 are always positive. Since r_1 and r_3 should be positive we have

$$r_1 > 0 \rightarrow w_1^3 - \frac{N_i}{2}r_f^3 > 0, \quad \text{and}$$
$$r_3 > 0 \rightarrow w_2^3 - \frac{N_i'}{2}r_f^3 > 0 \qquad (12a,b)$$

These expressions yield $U_f < 0.51$ and $U_f < 0.94$ for Model M_1, $U_f < 0.50$ and $U_f < 0.60$ for Model M_2, and finally $U_f < 0.66$ and $U_f < 0.43$ for Model M_3.

Also, we must have

$$r_2 < r_3 \rightarrow r_2^3 < r_3^3 \rightarrow w_1^3 - \frac{N_i}{2}r_f^3 < w_2^3 - \frac{N_i'}{2}r_f^3$$
$$r_4 < r_5 \rightarrow r_4^3 < r_5^3 \rightarrow w_2^3 + \frac{N_i'}{2}r_f^3 < \frac{N_i + N_i'}{U_f}r_f^3 \qquad (13a,b)$$

By substituting w_1 and w_2 from eqs. (4)–(6) and N_i', N_i for each case, we obtain that

$U_f < 0.07$ for M_1, $U_f < 0.18$ for M_2, and $U_f < 0.12$ for M_3.

This means that the proposed model is valid only for low-filler volume fractions.

Theoretical considerations

The theoretical analysis is based on the following assumptions:

(i) The inclusions and the matrix are elastic, isotropic, and homogeneous.
(ii) The inclusions have perfectly spherical shape.

(iii) The inclusions are large in number and their distribution is uniform so that the composite may be regarded as a quasi-homogeneous isotropic material.
(iv) The deformations applied to the composite are small enough to maintain linearity of stress–strain relations.

To find the relationships that give the expression for the elastic modulus, it will be assumed that classical theory of elasticity is applied to the representative volume element, whose mechanical properties equal the average properties of the composite and which can be represented by the previously described five concentric spheres. Let a pressure P_4 be applied on the outer surface of the sphere of radius e. Then, P_0, P_1, P_2, P_3, P_4 denote the interaction between different regions.

Because of the spherical symmetry, it is advantageous to use spherical coordinates (r,θ,φ). Of the three components of the displacement vector u_r, u_θ, u_φ only u_r is nonzero.

The solution to this problem can be approach by a stress function expressed by:

$$\Phi_i = \frac{C_i}{r} + D_i r^2 \tag{14}$$

where i varies from 1 to 5, which is the number of the phases.

To avoid infinite stresses at $r = 0$ for $i = 1$, the constant C_i must take the value of zero, i.e., $C_i = 0$. Then, the displacements are given from $\mathbf{u} = \frac{1}{2G_i}\text{grad}\Phi$:

$$u_{r,i} = \frac{1}{2G_i}\left(-\frac{C_i}{r^2} + 2D_i r\right) \tag{15}$$

with $u_{\theta,i} = u_{\varphi,i} = 0$, where G_i is the shear modulus of each phase.

The strains for each region can be determined from the following relationships:

$$\varepsilon_r = \frac{\partial u_r}{\partial r}, \quad \varepsilon_\theta = \frac{u_r}{r} + \frac{1}{r}\frac{\partial u_\theta}{\partial \theta}, \quad \varepsilon_\varphi = \frac{u_r}{r} + \frac{1}{r}\frac{\partial u_\varphi}{\partial \varphi}$$

Taking into consideration that $u_\theta = u_\varphi = 0$ and that $G_i = E_i/2(1 + v_i)$, where E_i is the elastic modulus and v_i is the Poisson ratio of each phase,

$$\begin{aligned} \varepsilon_{r,i} &= \frac{1+\nu_i}{E_i}\left(\frac{C_i}{r^3} + 2D_i\right) \\ \varepsilon_{\theta,i} = \varepsilon_{\varphi,i} &= \frac{1+\nu_i}{E_i}\left(-\frac{C_i}{r^3} + 2D_i\right) \end{aligned} \tag{16a,b,c}$$

The stresses for each region can be found from stress–strain relationships as follows:

$$\begin{aligned} \sigma_{r,i} &= \frac{2C_i}{r^3} + \frac{2(1+\nu_i)}{1-2\nu_i}D_i \\ \sigma_{\theta,i} = \sigma_{\varphi,i} &= -\frac{C_i}{r^3} + \frac{2(1+\nu_i)}{1-2\nu_i}D_i \end{aligned} \tag{17a,b,c}$$

The boundary conditions for the stresses are as follows:

$$\begin{aligned} \text{At} \quad r = r_i \quad &\rightarrow \quad \sigma_{r,i} = \sigma_{r,i+1} = -P_{i-1} \\ r = r_5 \quad &\rightarrow \quad \sigma_{r,5} = -P_4 \end{aligned} \tag{18}$$

Equations (17) applied to the above boundary conditions yield the values of the constants:

$$C_i = \frac{(P_{i-1} - P_{i-2})r_i^3 r_{i+1}^3}{2\left(r_{i+1}^3 - r_i^3\right)} \tag{19a,b}$$

$$D_i = \frac{\left(r_i^3 P_{i-2} - r_{i+1}^3 P_{i-1}\right)(1-2\nu_i)}{2\left(r_{i+1}^3 - r_i^3\right)(1+\nu_i)}$$

By substituting these values in eq. (15):

$$\begin{aligned} u_{r,i} = &-\frac{(P_{i-1} - P_{i-2})r_i^3 r_{i+1}^3(1+\nu_i)}{2\left(r_{i+1}^3 - r_i^3\right)E_i}\frac{1}{r^2} \\ &+ \frac{\left(r_i^3 P_{i-2} - r_{i+1}^3 P_{i-1}\right)(1-2\nu_i)}{2\left(r_{i+1}^3 - r_i^3\right)E_i} \end{aligned} \tag{20}$$

The boundary conditions must account for the continuity of displacements at the interfaces, i.e.,

$$\text{At} \quad r = r_i \quad \rightarrow \quad u_{r,i} = u_{r,i+1}$$

From which,

$$P_{i-1} = \lambda_{i-1} P_i \tag{21}$$

where

$$\lambda_i = 3r_{i+1}^3(r_i^3 - r_{i-1}^3(1-\nu_{i+1})E_i \Big/ \left\{ \begin{array}{l} \left[r_{i+1}^3(1+\nu_{i+1}) + 2r_i^3(1-2\nu_{i+1})\right](r_i^3 - r_{i-1}^3)E_i \\ +\left[r_{i-1}^3(1+\nu_i) + 2r_i^3(1-2\nu_i) - 3\lambda_{i-1}r_{i-1}^3(1-\nu_i)\right](r_{i+1}^3 - r_i^3)E_i \end{array} \right\} \tag{22}$$

Next, we substitute the obtained values of the constants [eqs. (19)] in eqs. (17) for the stresses and in eqs. (16) for the strains and we obtain:

$$\sigma_{r,i} = \frac{(P_{i-1} - P_{i-2}) r_{i-1}^3 r_i^3}{r_i^3 - r_{i-1}^3} \frac{1}{r^3} + \frac{r_{i-1}^3 P_{i-2} - r_i^3 P_{i-1}}{r_i^3 - r_{i-1}^3} \tag{23a,b}$$

$$\sigma_{\theta,i} = \sigma_{\varphi,i} = -\frac{(P_{i-2} - P_{i-1}) r_{i-1}^3 r_{i-1}^3}{2(r_i^3 - r_{i-1}^3)} \frac{1}{r^3} + \frac{r_{i-1}^3 P_{i-1} - r_i^3 P_{i-2}}{r_i^3 - r_{i-1}^3}$$

and

$$\varepsilon_{r,i} = \frac{(P_{i-1} - P_{i-2}) r_{i-1}^3 r_i^3}{(r_i^3 - r_{i-1}^3) E_i} \frac{1}{r^3} + \frac{r_{i-1}^3 P_{i-2} - r_i^3 P_{i-1}}{r_i^3 - r_{i-1}^3} \frac{(1 - 2\nu_i)}{E_i} \tag{24a,b}$$

$$\varepsilon_{\theta,i} = \varepsilon_{\varphi,i} = -\frac{(P_{i-1} - P_{i-2}) r_{i-1}^3 r_i^3 (1 + \nu_i)}{2(r_i^3 - r_{i-1}^3) E_i} \frac{1}{r^3} + \frac{r_{i-1}^3 P_{i-2}(1 - 2\nu_i) - r_i^3 P_{i-1}}{(r_i^3 - r_{i-1}^3) E_i}$$

The elastic modulus of the composite can be obtained by applying the energy balance to the spherical composite model. The strain energy of the composite must be equal to the sum of the strain energies of the five regions (phases) as follows:

$$\frac{1}{2}\int_{V_c} \frac{P_4^2}{K_c} dV_c = \frac{1}{2}\int_{V_1} \left(\sigma_{r,1}\varepsilon_{r,1} + \sigma_{\theta,1}\varepsilon_{\theta,1} + \sigma_{\varphi,1}\varepsilon_{\varphi,1}\right) dV_1 + \frac{1}{2}\int_{V_2} \left(\sigma_{r,2}\varepsilon_{r,2} + \sigma_{\theta,2}\varepsilon_{\theta,2} + \sigma_{\varphi,2}\varepsilon_{\varphi,2}\right) dV_2 + \cdots + \frac{1}{2}\int_{V_i} \left(\sigma_{r,i}\varepsilon_{r,i} + \sigma_{\theta,i}\varepsilon_{\theta,i} + \sigma_{\varphi,i}\varepsilon_{\varphi,i}\right) dV_i \tag{25}$$

where

$$K_c = \frac{E_c}{3(1 - 2\nu_c)} \tag{26}$$

is the bulk modulus of the composite and $dV = 4\pi r^2 dr$.

By substituting eqs. (23) for the stresses and eqs. (24) for the strain, after algebra we obtain the following relationship:

$$\begin{aligned}\frac{2(1-2\nu_c)}{E_c} &= 2\lambda_1^2\lambda_2^2\lambda_3^2\lambda_4^2 \frac{(1-2\nu_1)}{E_1} U_1 \\ &+ \frac{\lambda_2^2\lambda_3^2\lambda_4^2(1-\lambda_1)^2(U_1+U_2)U_1(1+\nu_2)}{E_2 U_2} \\ &+ \frac{2\lambda_2^2\lambda_3^2\lambda_4^2[\lambda_1 U_1 - (U_1+U_2)]^2(1-2\nu_2)}{E_2 U_2} \\ &+ \frac{(\lambda_3+\lambda_4)^2(1-\lambda_2)^2(1+\nu_3)(U_1+U_2+U_3)(U_1'+U_2)}{E_3 U_3} \\ &+ \frac{2\lambda_3^2\lambda_4^2[(U_1+U_2)\lambda_2 - (U_1+U_2+U_3)]^2(1-2\nu_3)}{E_3 U_3} \\ &+ \frac{(1-\lambda_3)^2\lambda_4^2(1+\nu_4)(1-U_5)(U_1+U_2+U_3)}{E_4 U_4} \\ &+ \frac{2\lambda_4^2[\lambda_3(U_1+U_2+U_3) - (1-U_5)]^2(1-2\nu_4)}{E_4 U_4} \\ &+ \frac{(1-\lambda_4)(1+\nu_5)(1-U_5)}{E_5 U_5} \\ &+ \frac{2[\lambda_3(1-U_5)-1]^2(1-2\nu_5)}{E_5 U_5}\end{aligned} \tag{27}$$

where the Poisson ratio of the composite, v_c, can be approximated by the inverse rule of mixtures as follows:

$$\frac{1}{\nu_c} = \frac{U_1}{\nu_1} + \frac{U_2}{\nu_2} + \frac{U_3}{\nu_3} + \frac{U_4}{\nu_4} + \frac{U_5}{\nu_5} \tag{28}$$

The volume fractions of the five regions according to the considered model are given as follows:

$$U_i = \frac{V_i}{V_c} = \frac{\frac{4}{3}\pi(r_i^3 - r_{i-1}^3)}{\frac{4}{3}\pi r_5^3} = \frac{r_i^3 - r_{i-1}^3}{r_5^3}, \quad i = 1,2,3,4,5 \tag{29}$$

For the thermal expansion coefficient, let us assume that ΔT is the increase in the temperature of the composite material. Also, we consider that only the first of the boundary conditions is valid in eq. (18), i.e., $P_4 = 0$ and

$$\text{At} \quad r = r_i \quad \rightarrow \quad \sigma_{r,i} = \sigma_{r,i+1} \tag{30}$$

These boundary conditions are applied to eqs. (17) for the stresses.

The boundary conditions for the continuity of the displacements at the interfaces can be expressed as follows:

$$\text{At} \quad r = r_i: \quad \varepsilon_{\theta,i+1} - \varepsilon_{\theta,i} = (\alpha_{i+1} - \alpha_i)\Delta T \tag{31}$$

where α_i denotes the thermal expansion coefficient of phase $i = 1$.

The solution of the system of equations yields the values of P_i.

$$P_i = L_i \Delta T \tag{32}$$

The thermal expansion coefficient α_c of the composite can be found using the following relation:

$$\left(\varepsilon_{\theta,5}\right)_{r=r_5} = (\alpha_5 - \alpha_c)\Delta T \quad \rightarrow \quad \alpha_c = \alpha_5 - \frac{\left(\varepsilon_{\theta,5}\right)_{r=r_5}}{\Delta T} \tag{33}$$

Noting that,

$$\alpha_2 = \alpha_4 = \alpha_f, \quad E_2 = E_4 = E_f, \quad \nu_2 = \nu_4 = \nu_f$$

and

$$\alpha_1 = \alpha_3 = \alpha_5 = \alpha_m, \quad E_1 = E_3 = E_5 = E_m, \quad \nu_1 = \nu_3 = \nu_5 = \nu_m$$

$$\alpha_c = \alpha_m - \left\{3(\alpha_m - \alpha_f)E_f(1 - U_5)(1 - \nu_5)\begin{bmatrix}\Theta\Lambda U_2(\Delta - AU_3) + (\Gamma A - B\Delta)\Lambda U_3 U_4 \\ -[(\Gamma A - B\Delta)H - \Theta AZ]U_4 U_5\end{bmatrix}\right\} \Big/ \{[(\Gamma A - B\Delta)H - \Theta AZ]K - I\Lambda(\Gamma A - B\Delta)\}U_5 \tag{34}$$

where

$$A = [(U_1 + U_2)(1 + \nu_2) + 2U_1(1 - 2\nu_2)]E_1 + 2U_2(1 - 2\nu_1)E_2$$

$$B = 3(U_1 + U_2)(1 - \nu_2)E_1$$

$$\Gamma = 3E_3U_3U_1(1 - \nu_2)$$

$$\Delta = 3E_2U_2(1 - U_4)(1 - \nu_3)$$

$$Z = E_2U_2[(1 - U_4)(1 + \nu_3) + 2(U_1 + U_2)(1 - 2\nu_3)] + E_3U_3[U_1(1 + \nu_2) + 2(U_1 + U_2)(1 - 2\nu_2)]$$

$$H = E_3U_3[(1 + \nu_4) + 2(1 - U_4)(1 - 2\nu_4)] + E_4U_4[(U_1 + U_2)(1 + \nu_3) + 2(1 - U_4)(1 - 2\nu_3)]$$

$$\Theta = 3E_4U_4(U_1 + U_2)(1 - \nu_3)$$

$$I = 3E_3U_3(U_1 + U_2 + U_3 + U_4)(1 - \nu_4)$$

$$K = E_4U_4\Big[(1 + \nu_5)(1 - U_5) + 2(U_1 + U_2 + U_3 + U_4)(1 - 2\nu_5)\Big] + E_5U_5\Big[(U_1 + U_2 + U_3)(1 + \nu_4) + 2(U_1 + U_2 + U_3 + U_4)(1 - 2\nu_4)\Big]$$

$$\Lambda = 3E_5U_5(U_1 + U_2 + U_3)(1 - \nu_4) \tag{35a–j}$$

The properties of the constituent materials that were used during the theoretical calculations are given in Table II.

Now, by using the previously described model, the elastic modulus, Poisson ratio, and thermal expansion coefficient can be evaluated for composites with low filler content.

The density of the composite can be calculated by the modified law of mixtures to include the five regions proposed by the model:

$$\rho_c = \rho_1U_1 + \rho_2U_2 + \rho_3U_3 + \rho_4U_4 + \rho_5U_5 \tag{36}$$

where ρ_i (i = 1,2,3,4,5) and ρ_c denote the density of the phases and composite, respectively.

EXPERIMENTAL PROCEDURE

The specimens used in the experiments consist of a matrix material, which is a cold-setting system based on a diglicidyl ether of bisphenol-A resin, cured with 8% triethylenetetramine, a hardener which is slightly lower than stoichiometry. One particle size of iron particles with average radius of 75 μm was used for all mixtures with filler volume fraction U_f = 0, 0.03, 0.05, 0.07, and 0.10.

The properties of the constituent materials are given as follows in the Table II:

- For the present investigation, composite specimens with a length of 0.30 m, a width of 0.10 m, and a thickness of 2×10^{-3} m were used during the tensile tests.
- Specimens of the same material were tested on a Du Pont 990 thermomechanical analyzer (TMA) to determine the linear thermal expansion

TABLE II
Properties of the Materials Used

Parameter	Iron	Epoxy resin
Elastic modulus, E (N/m^2)	210×10^9	3.5×10^9
Poisson ratio, ν	0.29	0.36
Density, ρ (kg/m^3)	7,800	1,190
Thermal expansion coefficient, α (°C^{-1})	15×10^{-6}	65.26×10^{-6}

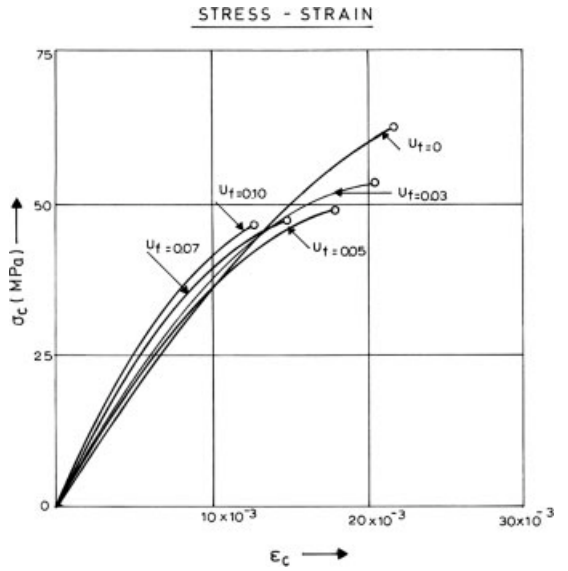

Figure 2 Stress–strain curves obtained from tensile experiments for various low filler contents.

coefficient. To determine the density, specimens of various filler contents with given volume were weighed in a sensible balance. By dividing the two values, the density was obtained. For the experiments concerning the qualitative explanations by correlating the macroscopic fracture behavior with microfailure behavior by means of the SEM, the fractured specimen surfaces were coated with a thin gold layer to enhance the image quality and to avoid charging phenomena. The fractographs were taken by a SEM (of type S4-10) of Cambridge Instruments.

RESULTS AND DISCUSSION

Figure 2 illustrates the variation of stress versus the longitudinal strain for various filler volume fractions of the iron particle-reinforced epoxy polymer as obtained from tensile experiments. From these curves, the effect of the low filler content on the mechanical behavior of the composite can be observed. The form of these curves shows that these composites generally present a nonlinearity. Because of high stress and strain concentrations in the regions around the particles, the elastic limit of the matrix is greater when compared with that of the composite. It is obvious that linear elastic behavior is observed only in the initial region of the stress–strain curves. From the same curves it can be seen that as filler content increases, a more extended elastic (time-independent) behavior results. This can be explained by the fact that the filler is a strongly elastic material and its presence weakens the viscoelastic (time-dependent) behavior of the matrix.

On the other hand, the nonlinear behavior of the stress–strain curves shown in Figure 2 can be in a great part explained by the existence of an interphase, which leads to a total or partial interruption of stress–strain continuity between matrix and inclusion. By this way, the elastic (time-independent) stress–strain transfer between matrix and particle is impeded, which means that only a increasing component of the time-dependent or viscoelastic stress–strain transfer can occur between matrix and particle. The previously proposed transfer mechanism can explain the observed appreciable nonlinear behavior with increasing particle volume fraction U_f. Thus, for instance, with increase in U_f there is also an increase in the net volume of the interphase which, as mentioned, tends to diminish the elastic stress–strain transfer. Thereafter, the corresponding increase of the elastic component due to the increase in the particle content cannot be optimally transferred from the particles into the matrix. In other words, the two concurrent mechanisms, i.e., the decrease in the elastic transfer efficiency and the relative increase in the viscoelastic component, the first one dominates and thus leads to the observed appreciable nonlinearity at higher volume fractions.

Figure 3 illustrates the variation of the tensile stress, σ_c and tensile strain ε_c at fracture versus filler content as obtained through experiments. It can be observed that the fracture stress decreases monotonically as the volume fraction increases, and that the experimental results are in good agreement with the theoretical values obtained from the expressions of Nicolais[28] and Nielsen[29] and Schrager[30] given by eqs. (A1), (A2), and (A3), respectively, in Appendix. As to the fracture behavior, it was observed[3] that the process of crack propagation is characterized by

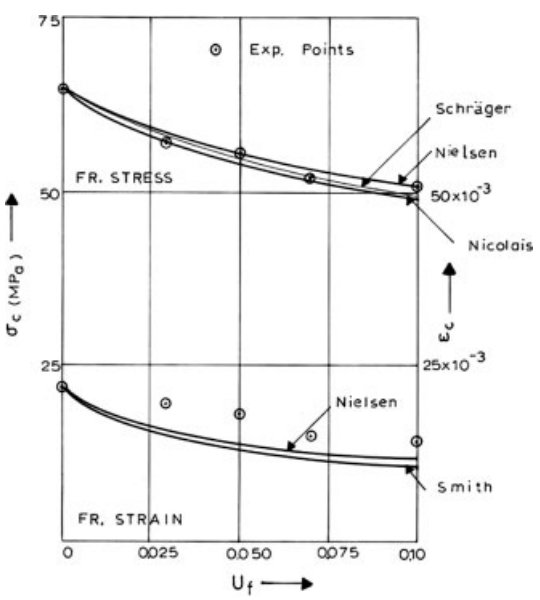

Figure 3 (a) Variation of the tensile stress at fracture of the composite versus filler content. (b) Variation of the tensile fracture strain of the composite versus filler content.

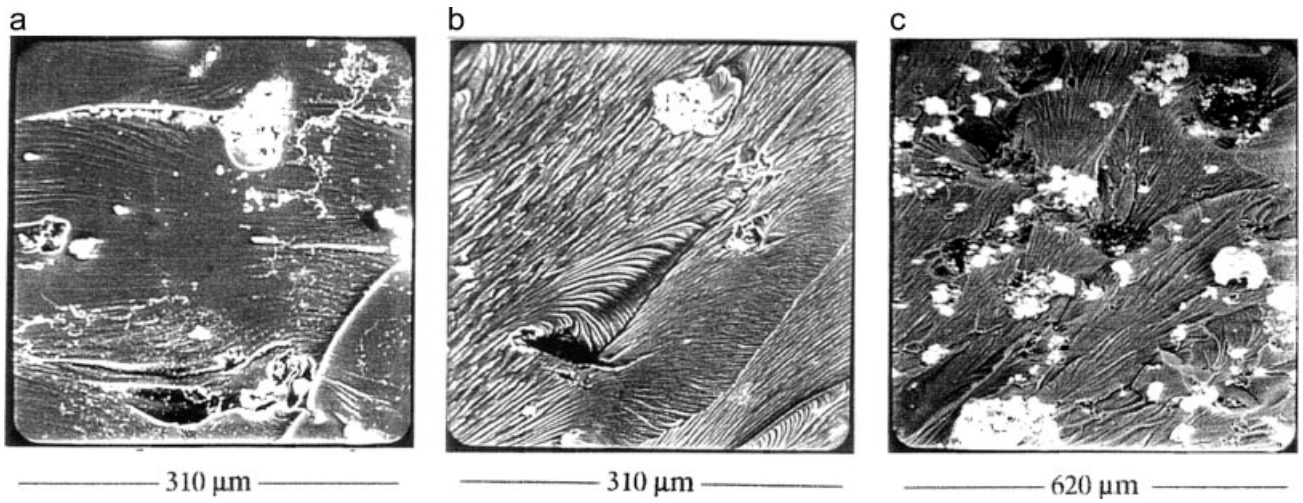

Figure 4 (a) Electron fractograph around inclusions "debonding (decohesion) gaps" due to the interphase are formed ($U_f = 0.03$), (b) electron fractograph with nonhomogeneous particle distribution and its strong local variation ($U_f = 0.10$), (c) electron fractograph with a strong "decohesion gap" between two close-spaced grains and the corresponding intense microplastic deformations ($U_f = 0.07$).

a fracture process zone (f.p.z.) developed at the crack tip. In the case of a composite material, the dimension of this f.p.z. when compared with the particle radius is a factor affecting the mode of crack propagation. In particular, when the particle radius is small as compared with the dimension of the f.p.z., the presence of the inclusion in the vicinity of the propagating crack tip modifies only the rheological behavior of the viscoelastic matrix while, at the same time, the particle size may not affect the path of the crack. On the contrary, when the filler particles are large, as compared with the dimensions of the f.p.z, then the presence of the filler particles may lead to a crack delay. Moreover, changes in the average properties of the highly strained material in the failure zone must be considered as a second phenomenon relating the changes in strength with filler particles, which are small as compared with the f.p.z. at the crack tip. The size of the f.p.z. is greatly affected by the presence of the finely dispersed particles. When the size of the f.p.z. increases then a microfracturing event takes place and this may lead to an increase in the fracture energy.

Moreover, the nature of the interfacial bond between matrix and filler particles is very important. In fact, perfect adhesion, corresponding to continuity of stresses and displacements at the interface, is a most common assumption for analytical treatments. However, with real composites this condition is very seldom fulfilled, and in addition, cracks, voids, and flaws extensively distort the stress/strain fields developed in the composite. Forms of imperfect bonding, depending either on the nature and/or the size of the particles or on the manufacturing process, as well as on the agglomeration of particles when extremely complex situations appear in the composite, is hardly susceptible to an analytical treatment. The earlier arguments are supported in a great part by the electron fractographs shown in Figure 4(a), where "decohesion gaps" between matrix and particles as well as conglomerations of them can be observed. This is an evidence of a poor adhesion strength at the interface. From Figure 4(b) one can further deduce tendency of an enhancement of the "debonding (decohesion) gaps" with increasing the grain size, which means an appreciable interaction between propagating crack and inclusions (grains). Further, from the Figure 4(c) it can be observed that for (very) close-spaced inclusions the "debonding gaps" are "modulated" with strong microplastic deformations that can be regarded as an evidence of the interinclusion interaction.

Figure 3 also illustrates the variation of the tensile fracture strain of the composite, ε_c, versus filler content as derived from the experimental results. It can be observed that the fracture strain decreases as filler volume fraction increases, because the addition of iron particles which are elastic material, in an epoxy resin, is a viscoelastic material, reduces its ductility even in low filler content of the particles. Thus, it is observed that the experimental results show a discrepancy with the theoretical values obtained from the expressions given by Smith[31] and Nielsen[32] in eqs. (A4) and (A5), respectively, in Appendix, and that the theoretical results are always below the experimental ones.

The theoretical values for Poisson ratio, elastic modulus thermal expansion coefficient, density, and the velocity of longitudinal waves are given in Table I.

Figure 5 illustrates the variation of the composite density ρ_c versus filler content as derived from the theoretical expression of eq. (36) together with the experimental results. A brief observation shows that

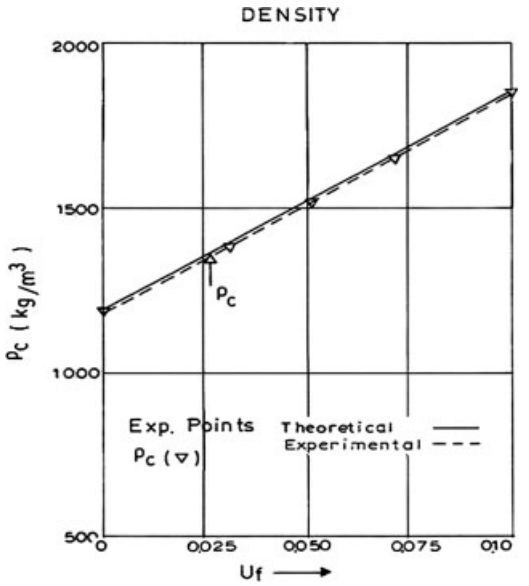

Figure 5 Variation of the composite density versus filler content.

there is a slight discrepancy between the two sets. Thus, it can be said that no appreciable inherent voids exist in the mass of the composite specimens.

In Figure 6, the variation of Poisson ratio, v_c, versus the filler content, U_f, is obtained from eq. (28). It can be observed that the Poisson's ratio decreases slightly when U_f is increased, which means that when adding iron particles in the epoxy polymer there is a reduction not only of the longitudinal strain as observed in Figure 3, something that would be expected since the iron particles are elastic whereas the epoxy resin is viscoelastic, but also a reduction of the transversal strain that leads to the decrease of Poisson ratio of the composite material.

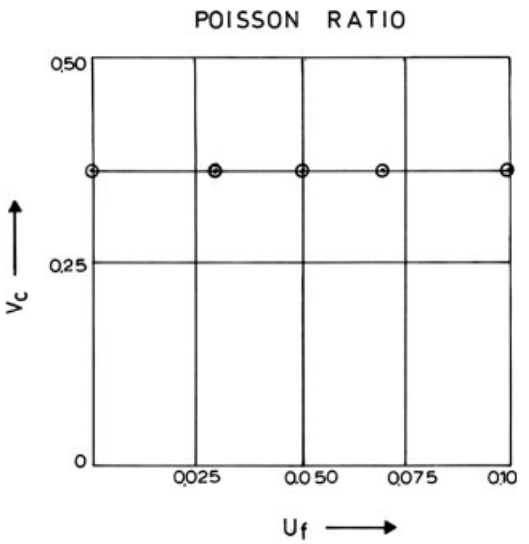

Figure 6 Variation of the Poisson ratio of the composite versus filler content.

Figure 7 illustrates the variation of the modulus, E_c, as derived from eq. (27) of the developed model together with eqs. (22) and (28) versus filler content. In the same figure, the theoretical curves derived from other theoretical expressions[33–38] given in Appendix [eqs. (A6)–(A11)] are also illustrated. All theoretical values of E_c increase with increasing the filler content. It can be observed that the theoretical values given by Counto [eq. (A9)], Einstein [eq. (A6)], and Takahashi [eq. (A11)] and especially by Paul [eq. (A7)] show great discrepancy with experimental results appearing in the same figure and derived by our experiments. The values derived from the two-phase model of Hashin et al.[6] and Kerner [eq. (A10)] are in good coincidence with experimental results, whereas the theoretical values derived from eq. (A8) of Guth-Smallwood[35,36] show a very good coincidence with experimental results for $U_f \leq 0.05$ but a discrepancy for higher values of U_f as the curve has abrupt rise. The theoretical values derived from the proposed model M_1 show some discrepancy with experimental results except for $U_f = 0.10$. The theoretical values derived from the proposed models M_2 and M_3 are in better coincidence with experimental results for $U_f < 0.10$. It can be seen that between those two models, the M_3 shows a slightly better agreement when compared with experimental values showing the influence of filler distribution. As to the form of the theoretical curves, those derived from the theoretical expressions of Einstein, Kerner, two-phase model, Takahashi and Guth-Smallwood present similarity since their concave part is upward, whereas those of Paul, Counto, and the proposed model have their concave part downward.

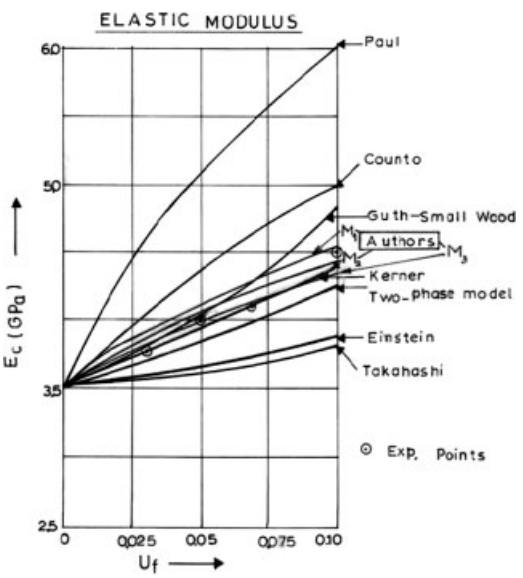

Figure 7 Variation of the elastic modulus of the composite versus filler content.

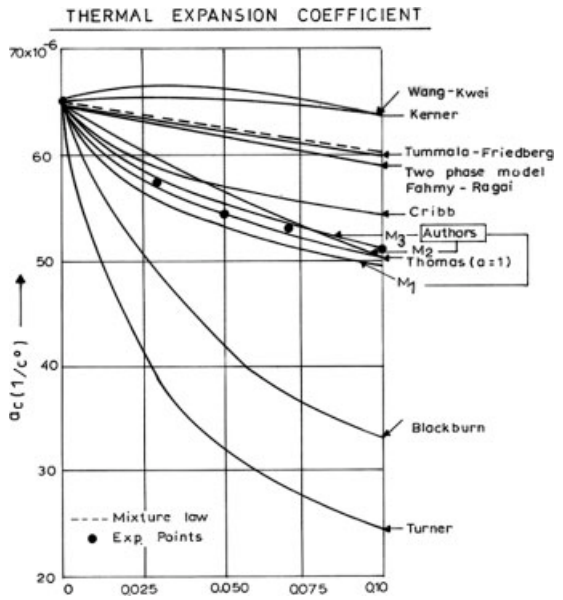

Figure 8 Variation of the thermal expansion coefficient of the composite versus filler content.

It is evident from the foregoing that it is difficult for the discussed models to predict the experimental data in an absolute manner because all theoretical assumptions cannot be fulfilled in the "real" material. Thus, for example, the assumption of equigranular particles, i.e., constant strain size cannot be valid as it can be seen from Figure 4(a–c). Rather, a strong degree of inequigranularity dominates. The assumption of a constant particle distribution cannot be valid either as it can be also seen especially from Figure 4(b). Rather, a strong local variation in this distribution can be stated. In this sense, it seems reasonable to assume that these two structural inhomogeneities may be among the principal sources of the observed discrepancies between the values derived from the models and experimental data concerning the elastic moduli.

Figure 8 illustrates the variation of thermal expansion coefficient of the composite α_c calculated by the aid of eq. (33) together with eqs. (35a–j) versus filler content U_f and together with theoretical expressions of other authors[17–20,22,24,26,27] given in eqs. (A12)–(A19) in Appendix, as well as with experimental results derived from our experiments, which were carried out on the composite material described in a previous section. As it can be observed, the majority of the theoretical curves show great discrepancies with the experimental results. Especially those given by Blackburn [eq. (A13)] and Turner [eq. (A12)] are far from the experimental values something that can also be said, to a lesser extent, for the theoretical values derived from the expressions given by Kerner [eq. (A14)], Wang and Kwei [eq. (A15)], Tummala–Friedberg [eq. (A16)], Fahmy–Ragai [eq. (A17)], the two-phase model, and mixture law. On the contrary, the experimental results are in fairly good agreement with the theoretical values derived from the expression of Cribb [eq. (A18)], Thomas [eq. (A19)], and the proposed models M_1, M_2, M_3. Among the proposed models, M_3 yields theoretical values which show less discrepancy with experiments. However, it should be pointed out that in the iron particle-filled epoxy polymers prepared in our laboratory, due to manufacturing conditions, agglomeration of particles may occur that can cause discrepancies, since the agglomeration of particles does not conform with basic assumptions of the theories concerned. Besides, disagreement between theoretical values and experimental results may be partly due to the quality of adhesion between matrix and fillers, which is an important factor and also to the size of the iron particles that can play a more pronounced role at low-filler volume fractions. Again, the previous arguments are supported by the fractographs in Figure 4(a–c), in which the previously mentioned structural inhomogeneities are revealed and which are responsible for the observed discrepancies between theory and experiment. In this context, it must be pointed out that this problem has been discussed in details in a previous study,[39] in which by means of a gross semiquantitative approach the strong effect of local variation in the grain distribution as well as the effect of the epoxy matrix heterogeneities, i.e., local variations in the matrix density on the thermomechanical behavior of the composite is revealed.

Finally, in the electron fractograph of Figure 4, where for $U_f = 0.07$, between two close spaced grains a strong "decohesion gap" with the corresponding intense microplastic deformations can be observed. This may be considered as an evidence for the existence of an interaction mechanism between the inclusions.

CONCLUSIONS

The effect of iron particles, although at low content, added into an epoxy matrix on mechanical and thermal properties were investigated. Measurements of the parameters concerned were carried out by means of tensile experiments and using a Du Pont 990 thermomechanical analyzer. Experimental results obtained for the tensile fracture strain and especially for the tensile fracture stress are in good agreement with those derived from existing theories, whereas those obtained for elastic modulus and thermal expansion coefficient are in good agreement only with the minority of existing theories. The theoretical values obtained from the proposed model are in good agreement with the experimental results for the thermal expansion coefficient and the elastic

TABLE A.I
Tensile Strength

Nicolais[28]	$\sigma_c = \sigma_m\left(1 - 1.21U_f^{2/3}\right)$	(A1)
Nielsen[29]	$\sigma_c = \sigma_m\left(1 - U_f^{2/3}\right)k$	(A2)
Schrager[30]	$\sigma_c = \sigma_m \exp(-rU_f)$	(A3)

TABLE A.II
Tensile Elongation

Smith[31]	$\varepsilon_c = \varepsilon_m\left(1 - 1.106U_f^{1/3}\right)$	(A4)
Bueche,[32] Nielsen	$\varepsilon_c = \varepsilon_m\left(1 - U_f^{1/3}\right)$	(A5)

modulus for model M_3 but at a lesser extent in agreement with those for models M_2, M_3, demonstrating the influence of particle distribution in the matrix on the elastic constants and thermal expansion coefficient. Also, certain theories assuming effective bounds for the elastic moduli of composites were not applicable in this case, since the large differences between the respective moduli of matrix and filler are pulling those bounds apart, and no accuracy can be obtained. On the other hand, some discrepancies between theoretical values and experimental results could be explained on a phenomenological basis. Structural inhomogeneities such as agglomerations of particles produced during the manufacturing and the nonuniform size of the inclusions revealed by SEM observations can play a more pronounced role at low-filler volume fractions.

APPENDIX

Theoretical expressions of the literature

Several theoretical or semiempirical equations for the elastic modulus and thermal expansion coefficient as well as for tensile strength and tensile elongation exist in the literature. Some of them are based on the theory of elasticity, some others use a mechanics of material approach or express a law of mixtures, and finally some of them try to match theoretical expressions to experimental data by appropriately defining the existing constants in these expressions.

In Table A.I, σ_m and σ_c denote the matrix and composite fracture stress, respectively, whereas k is a stress concentration factor, and r is a factor determined experimentally. Finally, U_f denotes the filler volume fraction.

In Table A.II, ε_c and ε_m denote the composite and matrix fracture strain, respectively.

TABLE A.III
Elastic Modulus

Einstein equation[33]	$E_c = E_m\left(1 + 2.5U_f\right)$	(A6)
Paul model[34]	$E_c = E_m\left[\dfrac{1 + (m-1)U_f^{2/3}}{1 + (m-1)\left(U_f^{2/3} - U_f\right)}\right]$	(A7)
Guth–Smallwood[35,36]	$E_c = E_m\left(1 + 2.5U_f + 14.1U_f^2\right)$	(A8)
Counto[37]	$\dfrac{1}{E_c} = \dfrac{1 - U_f^{1/2}}{E_m} + \dfrac{1}{\left(1 - U_f^{1/2}\right)U_f^{1/2}E_m + E_f}$	(A9)
Kerner[18]	$E_c = E_m\left[\dfrac{\frac{U_f G_f}{(7-5\nu_m)G_m + (8-10\nu_m)G_f} + \frac{U_m}{15(1-\nu_m)}}{\frac{U_f G_m}{(7-5\nu_m)G_m + (8-10\nu_m)G_f} + \frac{U_m}{15(1-\nu_m)}}\right]$	(A10)
Takahashi[38]	$\dfrac{E_c}{E_m} = 1 + (1-\nu_m)U_f \times \dfrac{E_f(1-2\nu_m) - E_m\left(1-\nu_f\right) + 10(1+\nu_m)E_f(1+\nu_m) - E_m(1+\nu_m)}{E_f(1+\nu_m) + 2E_m\left(1-2\nu_f\right) + 2E_f(4-5\nu_m)(1+\nu_m) + E_m(7-5\nu_m)\left(1+\nu_f\right)}$	(A11)

TABLE A.IV
Thermal Expansion Coefficient

Blackburn[19]	$\alpha_c = \alpha_f + \frac{\frac{3}{2}(1-\nu_f)U_m(\alpha_m-\alpha_f)}{\frac{1}{2}(1+\nu_f)+U_m(1-2\nu_f)+(1-2\nu_m)\frac{E_f}{E_m}U_f}$ (A12)
Turner[17]	$\alpha_c = \frac{U_m\alpha_m k_m + U_f\alpha_f k_f}{U_m k_m + U_f k_f}$ (A13)
Kerner[18]	$\alpha_c = \alpha_f U_f + \alpha_m U_m + U_f U_m(\alpha_m-\alpha_f)q$ (A14) with $q = \frac{\frac{1}{k_m}-\frac{1}{k_f}}{\frac{U_f}{k_f}+\frac{U_m}{k_m}+\frac{3}{4G_m}}$
Wang and Kwei[24]	$\alpha_c = \alpha_m - U_f q(\alpha_m-\alpha_f)$ (A15) with $q = \frac{\left(\frac{3E_f}{E_m}\right)U_f}{\frac{E_f}{E_m}[2U_f(1-2\nu_m)+(1+\nu_m)]+2U_m(1-2\nu_f)}$
Tummala–Friedberg[27]	$\alpha_c = \alpha_m - U_f q(\alpha_m-\alpha_f)$ (A16) where $q = \frac{\frac{1+\nu_m}{2E_m}}{\frac{1+\nu_m}{2E_m}+\frac{1-2\nu_f}{E_f}}$
Fahmi–Ragai[22]	$\alpha_c = \alpha_m - \frac{3U_f(\alpha_m-\alpha_f)(1-\nu_m)}{2(1-2\nu_f)(1-U_f)\frac{E_m}{E_f}+2U_f(1-2\nu_m)+(1+\nu_m)}$ (A17)
Cribb equation[26]	$\alpha_c = q_1\alpha_m + q_2\alpha_f$ (A18) where $q_1 = \frac{k_m(k_c-k_f)}{k_c(k_m-k_f)}$ and $q_2 = \frac{k_f(k_m-k_c)}{k_c(k_m-k_f)}$
Thomas[20]	$\alpha_c^a = \alpha_m^a U_m + \alpha_f^a U_f$ (A19) where $-1 \le a \le +1$

In Table A.III, E_c and E_m denote the elastic modulus of the composite and the matrix, respectively, and U_f the filler volume fraction.

In Table A.IV, eq. (A14), the parameter q denotes the deviation for mixture law, whereas eq. (A19) for the two limit values becomes the mixture law and the inverse mixture law, respectively.

References

1. Theocaris, P. S. "The Mesophase Concept in Composites", Polymers/Properties and Applications 11, Springer-Verlag (1987).
2. Papanicolaou, G. C.; Paipetis, S. A.; Theocaris, P. S. Colloid Polym Sci 1978, 256, 625.
3. Wang, W.; Jasiuk, I. J Comput Mater 1998, 32, 1391.
4. Nielsen, L. E. Mechanical Properties of Polymers and Composites; Marcel Dekker: New York, 1974; Vol. 2.
5. Huang, W.; Rokhlin, S. I. Mech Mater 1996, 22, 219.
6. Hashin, Z.; Shtrikman, S. J Mech Phys Solids 1963, 11, 127.
7. Hojo, Z.; Toyoshima, W.; Tamura, M.; Kawamura, N. Polym Eng Sci 1974, 14, 604.
8. Jasiuk, J.; Chen, J.; Thorpe, M. F. J Mech Phys Solids 1992, 40, 373.
9. Kryszewski, M.; Bak, G. W. Acta Phys Pol A 1997, 92, 1163.
10. Bhattarcharya, S. K.; Basu, S.; De, S. K. J Mater Sci 1986, 13, 219.
11. Hashin, Z. Mech Mater 1990, 8, 333.

12. Chouchaoui, C. S.; Benzeggagh, M. L. Compos Sci Technol 1997, 57, 617.
13. Maurer, F. H.; Sinha, R.; Jain, R. K. In Composite Interfaces; Ishida, H., et al., Eds.; North-Holland, 1986; p 367.
14. Benveniste, Y. Mech Mater 1985, 4, 197.
15. Aboudi, J. Comput Sci Technol 1987, 28, 2103.
16. Saber-Samandari, S.; Khatibi, A. A. Key Eng Mater 2006, 312, 199.
17. Turner, P. S. J Res Natl Bur Stand 1946, 37, 239.
18. Kerner, E. H. Proc Phys Soc B 1956, 69, 808.
19. Arthur, G.; Coulson, J. A. J Nucl Mater 1964, 13, 242.
20. Thomas, J. P. General Dynamics; Fort Worth, TX, 1960; p AD 287.
21. Schapery, R. A. J Comput Mater 1968, 2, 380.
22. Fahmy, A. A.; Ragai, A. I. J Appl Phys 1970, 41, 5108.
23. Hashin, Z. J Appl Mech 1962, 29, 143.
24. Wang, T. T.; Kwei, T. K. J Polym Sci A 1969, 2, 889.
25. Lombardo, N. Compos Sci Technol 2005, 65, 2118.
26. Cribb, L. Nature 1968, 220, 576.
27. Tummala, R. R.; Friedberg, A. L. J Appl Phys 1970, 11, 5104.
28. Nicolais, L. Polym Eng Sci 1971, 11, 194.
29. Nielsen, L. E. J Appl Polym Sci 1966, 10, 97.
30. Schrager, M. J Appl Polym Sci 1978, 10, 2379.
31. Smith, T. L. Rubber Chem Technol 1961, 34, 123.
32. Bueche, F. J Appl Polym Sci 1960, 4, 107.
33. Einstein, A. Ann Phys 1905, 17, 549.
34. Paul, B. Trans Numer Inst Mech Eng 1960, 36, 218.
35. Guth, G. J Appl Phys 1945, 16, 20.
36. Smallwood, H. M. J Appl Phys 1964, 15, 758.
37. Counto, R. Magn Concr Res 1964, 16, 129.
38. Takahashi, K.; Ikeda, M.; Harakawa, K.; Tanaka, K. J Polym Phys Ed 1978, 16, 415.
39. Sideridis, E.; Kytopoulos, V. N.; Kyriazi, E.; Bourkas, G. Compos Sci Technol 2005, 65, 909.